Vacuum insulation panels for refrigerators

Sankarshan Verma[a], Harjit Singh[a,1]

[a]Institute of Energy Futures, College of Engineering, Design and Physical Sciences, Brunel University London, Uxbridge UB83PH, UK

Abstract

Globally, the electrical energy consumption of domestic refrigerators is approximately 6% of the total consumed. Typically, refrigerators are insulated with materials, such as foams (thermal conductivity >20 mW m^{-1} K^{-1}). Alternatively, using Vacuum Insulation Panels (VIPs) (thermal conductivity < 7 mW $m^{-1}K^{-1}$) would significantly reduce their overall energy consumption and improve their energy efficiency index whilst maximising the usable inner volume. This paper reviews previous published research into VIPs covering core, envelope, heat transfer phenomena and ageing. The choice of core material significantly affects both the heat transfer coefficient and the overall cost of a VIP. To improve cost effectiveness and ageing properties, research has focused on the development of alternative core materials. This development requires a fundamental understanding of the effect of several interfering factors on the performance of VIPs. In this paper, these factors have been extensively reviewed and the results presented in a systematic manner. The factors are grouped into three sections viz. material properties (pore/particle size, particle's mechanical strength and conductivity), design properties (sealing pressure, compaction density) and operating conditions (mean operating temperature, relative humidity). The effect of each factor, on heat transfer modes, radiation and conduction, has been thoroughly discussed, along with the physics involved, by objectively reviewing studies reporting these.

[1] Corresponding author. Tel.: +44 (0)1895 265468
E-mail address: harjit.singh@brunel.ac.uk

Keywords: Vacuum Insulation Panel, VIP, Thermal conductivity, Refrigerator, Ageing, Thermo-physical properties

Highlights

- Review paper covering the engineering and material science involved in vacuum insulation panels (VIPs) relevant to refrigerators.
- The factors affecting solid, gaseous and radiative conductivity are discussed in detail.
- VIP thermal conductivity testing, ageing mechanisms and commercially available VIPs are described.

Nomenclature

A: proportionality consant

D: mean pore size [m]

d_g: diameter of gas molecule [m]

d: diameter of particle [m]

E_R: Rosseland mean specific extinction coefficient [m^{-1}]

k_B: Boltzmann constant [JK^{-1}]

k_{eff}: effective thermal conductivity [$mWm^{-1}K^{-1}$]

k_{evac}: thermal conductivity of fully evacuated VIP [$mWm^{-1}K^{-1}$]

k_g^0: gaseous conductivity of free gas [$mWm^{-1}K^{-1}$]

k_{gR}^0: reduced gaseous conductivity of free gas ($k_{gR}^0 = \frac{k_g^0}{\Lambda}; \Lambda = 4.36$ $mWm^{-1}K^{-1}$) [$mWm^{-1}K^{-1}$]

k_g: gaseous thermal conductivity [$mWm^{-1}K^{-1}$]

k_p: thermal conductivity of a particle [$mWm^{-1}K^{-1}$]

k_r: radiative conductivity [$mWm^{-1}K^{-1}$]

k_s: solid thermal conductivity [$mWm^{-1}K^{-1}$]

k_w: thermal conductivity due to moisture in the VIP core [$mWm^{-1}K^{-1}$]

l_g: molecular mean free path length [m]

$m_{VIP,dry}$: mass of dry VIP core [kg]

N: normalization constant in Reichenauher's model

n: refractive index

p: pressure [Pa]

p_i: initial pressure of gas inside VIP [Pa]

$p_{1/2}$: critical pressure [Pa]

T: mean temperature [K]

T_R: reduced temperature ($T_R = \frac{T}{T_c};\ T_c = 132.5\ K$) [K]

$\frac{T_m \cdot p_0}{T_0}$: conversion factor from standard (index 0) to measurement conditions (index m) [Pa]

V_{eff}: pore volume of core material [m^3]

X_w: percent of water contained inside the core

Greek symbols

β: constant used in gaseous conductivity calculation

ρ: density [kg m^{-3}]

σ_p: spread of a Gaussian distribution

σ: Stefan-Boltzmann constant [$Wm^{-2}K^{-4}$]

φ_i: contribution of i^{th} pore towards total porosity

φ_o: ambient relative humidity

Abbreviations

AF: Aluminium foil

ATR: Air transmission rate

MF1, MF2: Aluminium coated multi-layer foils

$W/MVTR$: Water or Moisture vapour transmission rate

PU: Polyurethane

VIP: Vacuum Insulation Panel

FTIR: Fourier Transform Infrared

1. Introduction

Refrigeration accounts for around 15% of the total energy consumption in a household (IIR, 2009) consuming 6% of the total electrical energy produced worldwide (Negrão and Hermes, 2011). Approximately 50% of the cooling load stems from the heat transmitted through the refrigerator walls (ASHRAE, 2006), see figure 1. Integration of Vacuum Insulation Panels (VIPs) in refrigerators' walls would drastically reduce the overall *U*-value due to their low thermal conductivity (k < 7 mW m^{-1} K^{-1}). Figure 2 compares the thermal conductivity of a VIP with conventional insulation materials used in refrigerator walls.

Table 1 lists the previous studies reporting, the usage of VIPs in refrigerators and the corresponding reduction in energy consumption. Thiessen et al. (2016) reported a 21% reduction in energy consumption when 56% of the refrigerator area was covered with VIPs in place of polyurethane (PU) foam. Also, their study revealed that insulating the rear wall of the refrigerator is more effective than insulating the side walls. Tao et al. (2004) reported a 29% decrease in energy consumption of a display case refrigerator when the walls were insulated with PU foam core VIPs and the front door was vacuum glazed. Hammond and Evans (2014) predicted a payback period of 9.7 years for fridges and 4.5 years for freezers using VIPs (thermal conductivity: 4 mW m^{-1} K^{-1}) costing £38 m^{-2} compared with PU foam. Yusufoglu (2013) performed reverse heat leak tests reporting a 26% decrease in energy consumption when a 250 litre freezer was insulated with 25 mm thick VIPs with a thermal conductivity of 5 $mWm^{-1}K^{-1}$. Energy consumption decreased to 30% when a 400 litre refrigerator was insulated with VIPs with a thermal conductivity of 4.5 mW m^{-1} K^{-1}. Trias et al. (2018), using their mathematical model (temperature difference: 45-53 °C in freezer, 20-28 °C in freezer), predicted that the energy efficiency index of a domestic refrigerator-freezer would upgrade from 42 (A+ category) to 18.54 (A+++ category) when VIPs were embedded in the four

fridge walls and freezer door. A study by the authors (Verma and Singh, 2019a) reported an energy consumption reduction of 19.6% and a rise in inner volume by 32% when fumed silica VIPs were used as an insulation in a domestic refrigerator sidewalls. The application of VIPs has been explored in other cold chain equipment as well, for example the internal volume of a reefer truck will increase by approximately 3% by using VIPs instead of PU foam (Verma and Singh, 2019b).

Table 1: Summary of studies with VIP used as refrigerator insulation.

Study	VIP core	Thermal conductivity ($mW\ m^{-1}\ K^{-1}$)	Testing / modelling conditions		Energy consumption reduction (%)
			Compartment temperature (°C)	Ambient temperature (°C)	
Thiessen et al. (2016)	Fibre glass	-	-	18	21% reduction with 56% wall area VIP insulated
Tao et al. (2004)	PU foam	8	48	0	28.9
Hammond and Evans (2014)	-	4	5 (fridge) -20 (freezer)	25-30	48.7
Yusufoglu (2013)	-	4.5	5.2	25.2	30

(Verma and Singh, 2019a)	Fumed silica	3.7 (changing with age)	5 (fridge) -20 (freezer)	25-30	19.6	(over lifetime)

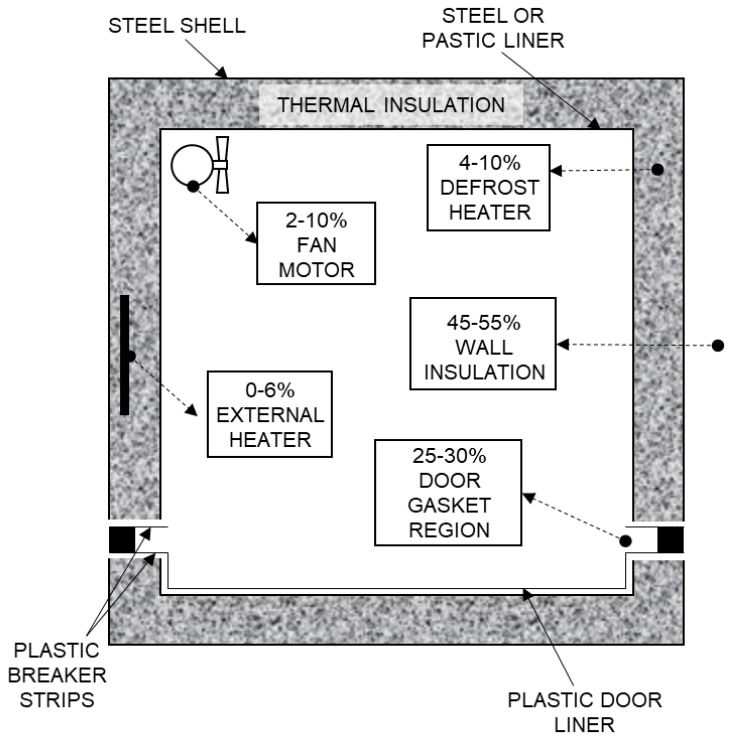

Fig. 1: Refrigerator cabinet cross-section showing different cooling loads. Adapted from (ASHRAE, 2006).

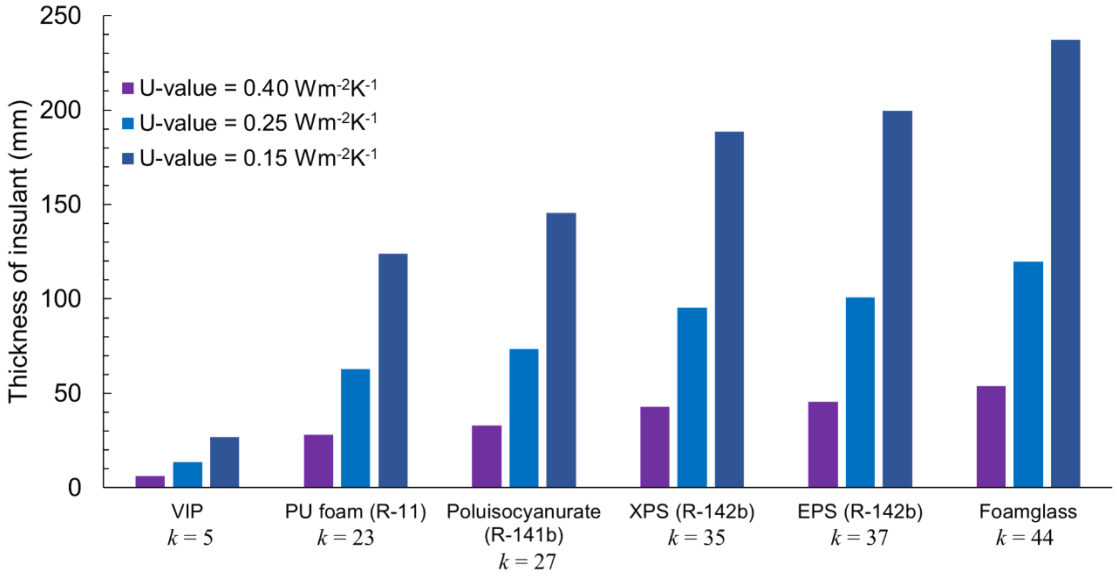

Fig. 2: Thermal conductivity of various insulating materials. The *k*-value represents the thermal conductivity in mW m^{-1} K^{-1}. Adapted from (ASHRAE, 2006).

The benefits of using VIPs in refrigerators have been well established. However, VIPs face obstacles in being the insulation of choice in refrigerators due to a variety of factors such as: i) uncertainty over an assured thermal conductivity, ii) uncertainty over the lifetime of the VIPs, iii) uncertainty over a constant supply of VIPs if their demand ramps up and iv) the high cost of VIPs, which can be five times per unit area higher than conventional foam insulation.

To overcome the above-mentioned challenges, it is necessary to understand the thermo-physical phenomena occurring in VIPs, to develop new core and envelope materials with improved properties leading to a longer lifetime and a reliable performance at lowest possible cost. This information is scattered over vast published literature which can at times be ambiguous and even contradictory. In the present paper, all thermal phenomena relevant to VIPs have been consolidated and critically reviewed.

2. Heat transfer phenomena in a VIP

In materials with high porosity (75% - 99%) such as foams, powders and fibres, the overall thermal conductivity is influenced greatly (50-70%) by the thermal conductivity of the gas trapped in the pores (Kuhn et al., 1992; Placido et al., 2005). Due to the suppression of gas conduction, the effective thermal conductivity of an evacuated porous material could be reduced by three to four times compared to its un-evacuated state. This is the principle of vacuum insulation panels wherein a highly porous open pore material is evacuated to a low pressure (0.01-10 mbar) and sealed in a multilayer envelope with low gas and water vapour permeation.

Other than convection, all modes of heat transfer i.e. solid conduction, gaseous conduction and radiation, simultaneously exist in an evacuated VIP core. These modes can be assumed to

act in parallel paths, the effective thermal conductivity of an evacuated VIP core can be expressed by equation (1).

$$k_{eff} = k_s + k_g + k_r \#(1)$$

The thermal performance of a VIP depends on a range of factors which are summarised in

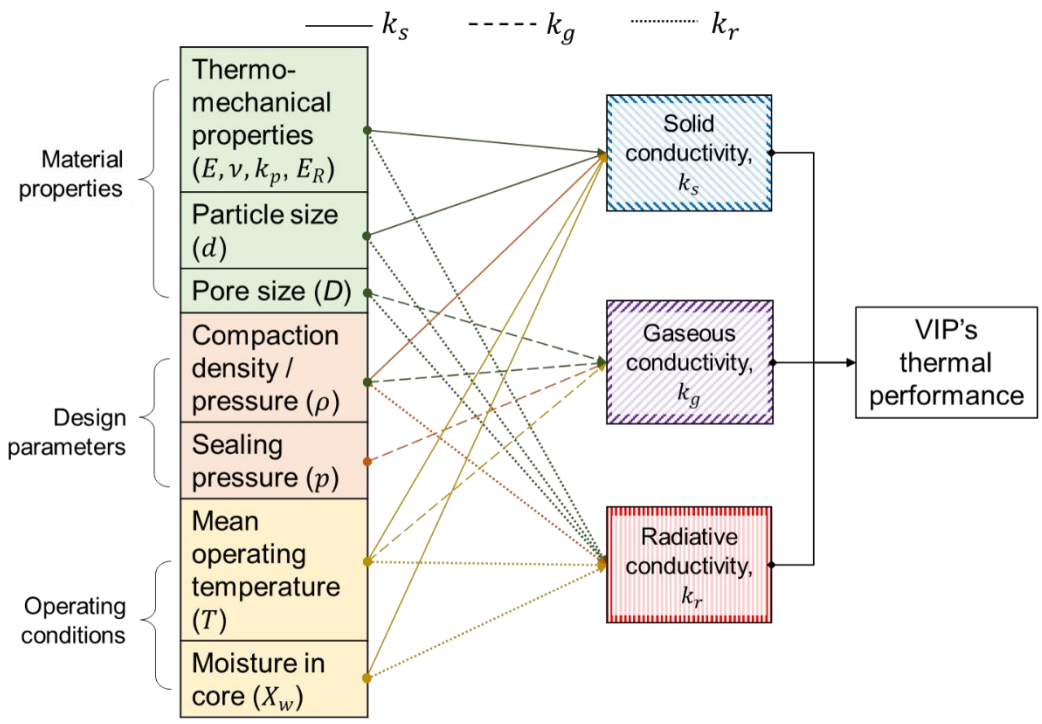

Fig. 3: Factors affecting the thermal performance of a VIP.

figure 3 and discussed in the following sections.

2.1 Material properties

Material properties which affect the thermal performance of a VIP core include: i) thermo-mechanical properties, such as elastic modulus (E), Poisson's ratio (ν), particle's thermal conductivity (k_p), extinction coefficient (E_R) ii) particle size (diameter for both spherical and cylindrical particles) and iii) pore size. Pores are either the voids between any two neighbouring particles (inter-particle pores) or the ones present on the surface of particles

(intra-particle pores). Generally, pore shapes are assumed as cylindrical and pore size defined as the diameter of these cylinders (Webb, 1993).

2.1.1. Effect of thermo-mechanical properties

Glass based materials like glass fibres and silica powders (fumed silica, silica aerogel etc.) contain ~99% Silicon dioxide (or SiO_2), whereas perlites are ~85% SiO_2 (the rest being metallic oxides like Na_2O, Al_2O_3 etc.). The chemical composition of a material describes its lattice structure and thus the conductive heat transfer through a particle (k_p). Due to their lattice structure, amorphous silica based materials, such as fumed silica, glass fibres, silica aerogels, are favoured for VIP core material.

The conductive heat transfer in materials, such as powders and fibres, occur through the point/area of contact between neighbouring particles. During core manufacturing, compressive forces either deform the particles, thus increasing the area of contact between these or cause re-packaging of particles, bringing them close to each other and consequentially the heat transferred from one particle to another increases. Clearly, particles' mechanical properties such as elastic modulus (E) and Poisson's ratio (ν), affect solid conduction. Kwon et al. (2009) developed analytical models for solid conduction in powdery, foamy and fibrous materials. The models for foamy and fibrous materials returned values sufficiently close to experimental results, however, the one for powders has unacceptably high deviation and thus, requires improvement (Verma and Singh, 2019b).

Heat transferred via infrared radiation (IR), 2.5 μm – 15 μm, is attenuated differently by different materials. For example, SiO_2 strongly attenuates IR radiation above the wavelength range of 7.5 μm but allows a radiation leakage in the wavelength range of 4-7 μm (see figure 4). Silicon Carbide (SiC), on the other hand, strongly attenuates IR radiation below 7 μm above 10 μm. The attenuation of IR radiation induces a decrease in radiative conductivity. The overall radiative conductivity (k_r) of a sample with large optical thickness and isotropic

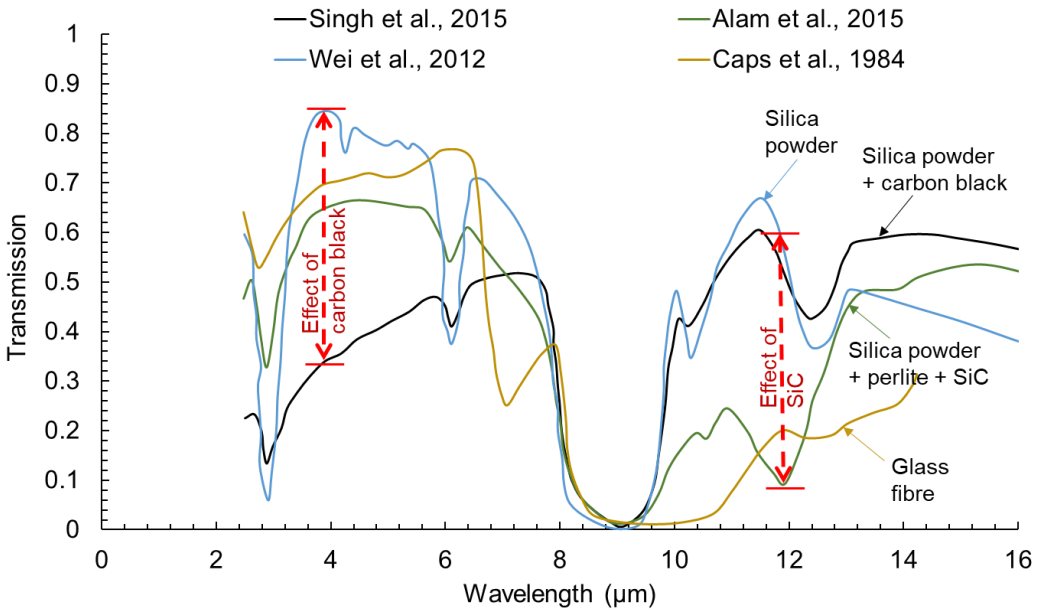

Fig. 4: Infrared waves' transmission from various materials. Dotted arrows show the decreased transmission from silica powders due to addition of opacifiers.

scattering is calculated using a diffusion approximation, as shown in equation 2, (Deissler, 1964).

$$k_r = -\frac{16\sigma n^2 T^3}{3E_R} \#(2)$$

The term E_R is called the overall extinction coefficient which defines the ability of a material to attenuate incident radiation. In order to increase the extinction coefficient (or decrease the IR transmission), as shown in figure 4, opacifiers, such as carbon black and silicon carbide, are employed. For instance, the addition of carbon black in silica powder decreases the IR

transmission in near IR wavelength region (2.5-8 μm) whereas the effect of addition of silicon carbide is more prominent in the far IR region (9-14 μm). These opacifiers therefore reduce the overall heat transfer through IR radiation in core materials. The extinction coefficient (E_R) is affected by the particle size and mean operating temperature (as discussed in further sections 2.1.2 and 2.3.1) and can be calculated using the following three methods:

a) Calorimetric measurements

Thermal conductivity of a fully evacuated insulant is measured as a function of temperature and is plotted with T^3. Regression analysis can then be performed to separate out the effective solid conductivity, provided its variation with temperature is known. The slope of the curve can be compared with equation (2) to calculate the extinction coefficient (E_R). This method has been used by several researchers including Caps et al. (2001) and Caps and Fricke (2000). However, this method doesn't account for the temperature dependence of the extinction coefficient.

b) Infrared transmission measurements

Infrared transmission is measured using FTIR spectrophotometer. Foams can be tested directly by making pellets and powders can be tested by mixing them with KBr in pellets. The spectral transmission thus obtained is converted to E_R using Beer-Lambert's law and Rosseland mean diffusion (Alam et al., 2014; Kuhn et al., 1992; Wei et al., 2011).

c) Mie scattering theory

If the index of refraction (n) and the particle geometry is known, the extinction coefficient can be calculated by employing Mie scattering theory, which describes the scattering of an electromagnetic plane wave due to spherical particles (as in fumed silica and perlites) or infinite cylinders (as in fibres). Mie theory predicts

the relative cross-sections, or coefficients of extinction, absorption and scattering. Several researchers have used Mie theory to optimize opacifier properties such as material, particle size, density (Caps et al., 1984; Liang et al., 2017; Napp et al., 1999; Wang et al., 2013; Zhu et al., 2018).

The calorimetric method requires extensive experimentation and doesn't take into account the temperature dependence of E_R. The Mie scattering theory method, though is computationally complex, is highly preferred because it requires minimum inputs, besides taking into account the effect of particle sizes on E_R.

2.1.2. Effect of particle size

The attenuation of IR waves occurs both due to absorption and scattering by the particles. Absorption depends on the type of material, based on difference in lattice structures and free electrons, whereas the scattering depends on both, the type of material as well as particle size. Napp et al. (1999) used Mie scattering theory to optimise the particle size of silicon carbide, used as an opacifier in silica powder, for maximum IR extinction to minimise the amount of radiative heat transferred. It was reported that for SiC particles with sizes ranging from d = 3 to 5 μm caused a maximum extinction at room temperatures. Wang et al. (2013) reported that this optimum opacifier particle size is also the function of mean operating temperatures; for SiC it's d = 6 μm for T<500K, d = 5 μm for 500K<T<800K and d = 4 μm for T> 800K. Recently, Mie scattering theory has been used to design new spherical core/shell opacifiers consisting of carbon cores and $SiC/TiO_2/Al_2O_3$ shells for low density and high temperature insulation (Zhu et al., 2018).

Particle size also describes the solid conductivity. Solid conduction of particulate material is not the same as the bulk material; for instance, solid conduction of fumed silica is 4 mW m^{-1} K^{-1} (Caps et al., 2001) whereas that of an individual silica particle (the bulk

material) is approximately 1500 mW m^{-1} K^{-1}. Every particle to particle contact can be understood as a thermal resistance higher than that offered by the particle itself. For core particles with similar morphology, smaller particle size gives rise to higher number of contacts and hence lower a solid conductivity value. This is the reason why perlites (particle size 10-100 µm) have higher solid conductivity than fumed silica (particle sizes 0.002-0.01 µm). A modified phonon model developed by Bi and Tang, (2013) takes into account the particle size to calculate the solid conductivity. For aerogels, the model predicted a solid conductivity rise of approximately 50% when particle diameter increased from 5 nm to 500 nm. This model has been experimentally validated for aerogels (silica and carbon), but not for other VIP core materials, such as perlites or glass fibres. The experimental study by (Kaganer, 1969) shows the effect of particle size on the thermal conductivity for silica powders and perlites, see figure 5. As shown in figure 5, there exists an optimal particle size based on which the radiation and solid conduction through the particles is minimum. The optimum particle size for silica and perlites lie between d = 10 and 100 µm.

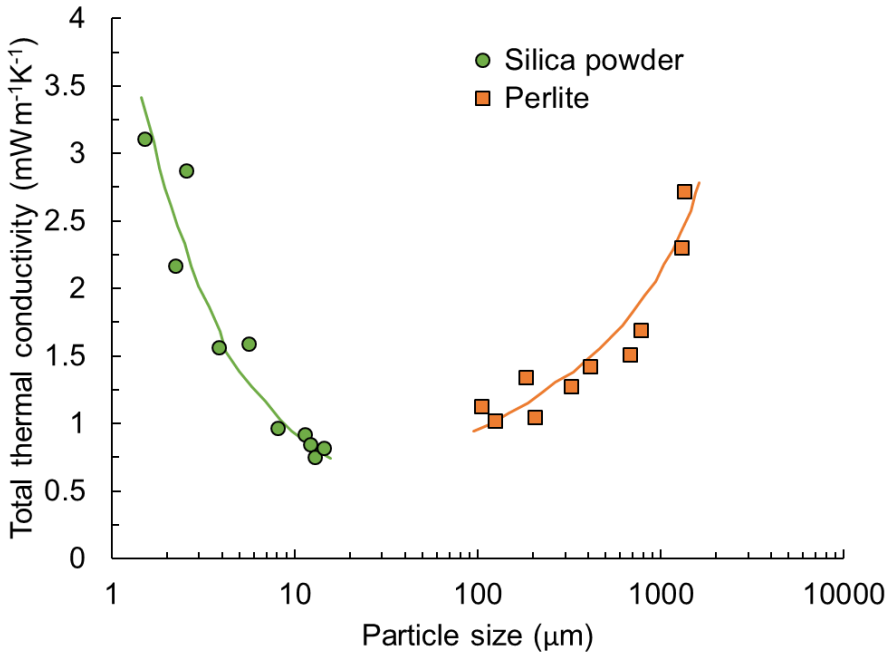

Fig. 5: Effect of particle size on the thermal conductivity of evacuated silica powder (T = -81 °C) and perlite (T = 23.5 °C). Adapted from (Kaganer, 1969).

2.1.3. Effect of pore size

The presence of gas inside the pores causes heat transferred by conduction when there is a collision between any two neighbouring gas molecules separated by a distance at least equal to the mean free path of gas, under the prevailing thermodynamic conditions, see figure 6. However, when the size of the pores is smaller than the mean free path length, according to the Knudsen effect, the molecules hit the pore walls instead of colliding with each other and conduct no heat. Figure 7 shows the average pore sizes of various materials taken from various sources (Chen et al., 2015; Kim et al., 2012; Lee et al., 2002; Reichenauer et al., 2007; Zhang et al., 2012). The mean free path length of air at room conditions (25 °C, 1 atm) is approximately 0.01 μm and is shown as the vertical dotted red line in figure 7. Closer is the mean free path length to the average pore size, lower will be the gaseous conductivity. Thus, materials with smaller pore sizes, like silica aerogels have very a low gaseous conductivity.

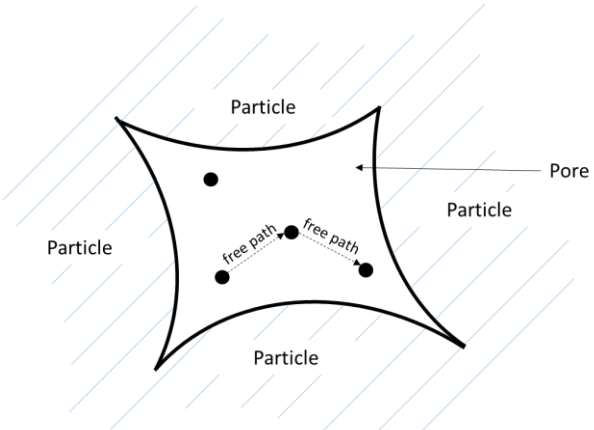

Fig. 6: A schematic of gaseous conduction inside the pores.

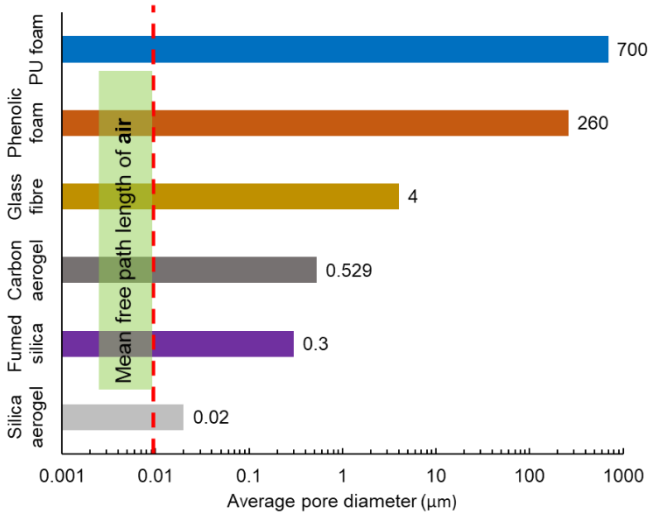

Fig. 7: Average pore diameters of various materials and the mean free path length of air at 1 atm pressure.

However, at the same time, they must be highly porous to minimise the heat transfer through solid conduction.

A simple analytical model to calculate the heat transfer by gaseous conduction between two parallel plates was modified by Kaganer (1969) to estimate the heat conducted by gas in a pore. In the modified model, the gap between the plates was replaced by pore size (equation 3).

$$k_g = \frac{k_g^0(T)}{1 + 2\beta \frac{l_g(p,T)}{D}} \#(3)$$

The pore structure of insulants, however, is complex with pore sizes differing by an order of 100 in the same material (see figure 8). Thus, using one single value to calculate the gaseous conduction could produce erroneous results. Kaganer (1969) approximated the complex pore structure of the insulants with pores of two sizes, corresponding to the mean dimensions of the inter-granular spaces and the micro-pores on the grains. As a result, equation 4 was proposed to calculate gaseous conductivity.

$$k_g = \frac{k_1}{1 + \frac{2\beta l_{g1}}{D_1}} + \frac{k_2}{1 + \frac{2\beta l_{g2}}{D_2}} \#(4)$$

where D_1 is the mean pore size of inter-particle pores and D_2 for the intra-particle pores and k_1 and k_2 are material specific constants. As per Kaganer's assumptions, D_1 is the abscissa of the intersection of the cumulative intrusion curve with a horizontal line drawn at 75% porosity value and D_2 is one third of D_1. Further, the values of k_1 and k_2 could be calculated for a given insulant using the experimental values of thermal conductivity under high vacuum and at atmospheric pressure.

Reichenauer et al. (2007) correlated the values of k_1 and k_2 to the porosities caused by inter and intra-particle pores (φ_1,φ_2) and found a good agreement between experimental and analytical values by using equation (5, 6)

$$k_1 = \varphi_1 \times k_g^0 \#(5)$$

$$k_2 = \varphi_2 \times k_g^0 \#(6)$$

Reichenauer et al. (2007) further developed the model to account for the contribution of every pore size, by calculating the value of φ for each pore size, see equation (7).

$$k_g = \frac{1}{N} \int \exp\left(-\frac{1}{2}\frac{(D'-D)^2}{{\sigma_p}^2}\right) \frac{k_g^0}{1+\frac{2\beta l_g}{D'}} dD' \#(7)$$

Though more accurate, the difference between the results from the two-pore model (equations 4, 5, 6) and full pore size model (equation 7) was meagre for the materials tested. Also, the model's equations were difficult to solve analytically. The model was simplified and improved by Bi et al. (2012), who numerically solved the equation (7) and proposed modifications to account for larger pores, see equation 8, 9, assuming that pore size distribution followed a Gaussian trend. The model presented a good approximation for gaseous conductivity for aerogel, but the reason for multiplying φ_i with two in the range of $[D+\sigma_p, D+3\sigma_p]$ needs more analytical proof (equation 9).

$$k_g = \sum_{i=1}^{n} \varphi_i \frac{k_g^0}{1+\frac{2\beta l_g}{D_i}} \#(8)$$

$$\varphi_i = \begin{cases} \frac{\Delta D}{\sqrt{2\pi}\sigma_p} e^{-\frac{(D_i-D)^2}{2{\sigma_p}^2}} & D_i \in [D-\sigma_p, D+\sigma_p] \; D_i - \sigma_p > 0 \\ \frac{2\Delta D}{\sqrt{2\pi}\sigma_p} e^{-\frac{(D_i-D)^2}{2{\sigma_p}^2}} & D_i \in [D+\sigma_p, D+3\sigma_p] \end{cases} \#(9)$$

If the pore size distribution of a material is known, which is required to calculate the parameter σ_p in equations 7 and 9, the gaseous conductivity can be calculated by equation (10), as suggested by Bi et al. (2012).

$$\varphi_i \approx \frac{f(D_i)}{\sum_{j=1}^{j_{max}} f(D_j)\Delta D_j} \#(10)$$

Characterization tests like Mercury Intrusion Porosimetry (MIP) and nitrogen adsorption techniques can be used to measure the distribution of pore sizes in a porous material. MIP, although changes the pore structure due to buckling of particles under compressive forces exerted by intruding mercury, is used because of the wide range of pore sizes that can be measured. Besides, the results provided by pore size distribution analysis can be interpreted in different ways. For example, Bi et al. (2012) have used the differential intrusion plots and Chang et al. (2016) the log differential intrusion as pore size distribution. Chang et al. (2016)'s results along with the corresponding calculated differential intrusion are presented in figure 8, which shows that differential intrusion results could present an incomplete picture, as it doesn't take into consideration large inter-particle pores (pore size>0.05 μm). In conclusion, one can say that use of differential intrusion for materials which have small pores and narrow pore size distribution, for example aerogel, is justifiable, but for materials with wider pores size distribution, for example fumed silica and perlites, a logarithmic differential intrusion should be used alternatively.

Current models are capable of calculating the gaseous conductivity provided the pore size distribution of the material is available. The pore size distribution is affected by the compaction density and composition of the mixture.

Pores affect the radiative transfer as well. For instance, the grains of perlites contain large pores which produce relatively strong scattering of infrared radiation. The radiative transfer through perlite is hence 1.5 times lower than that of aerogel of same density and thickness

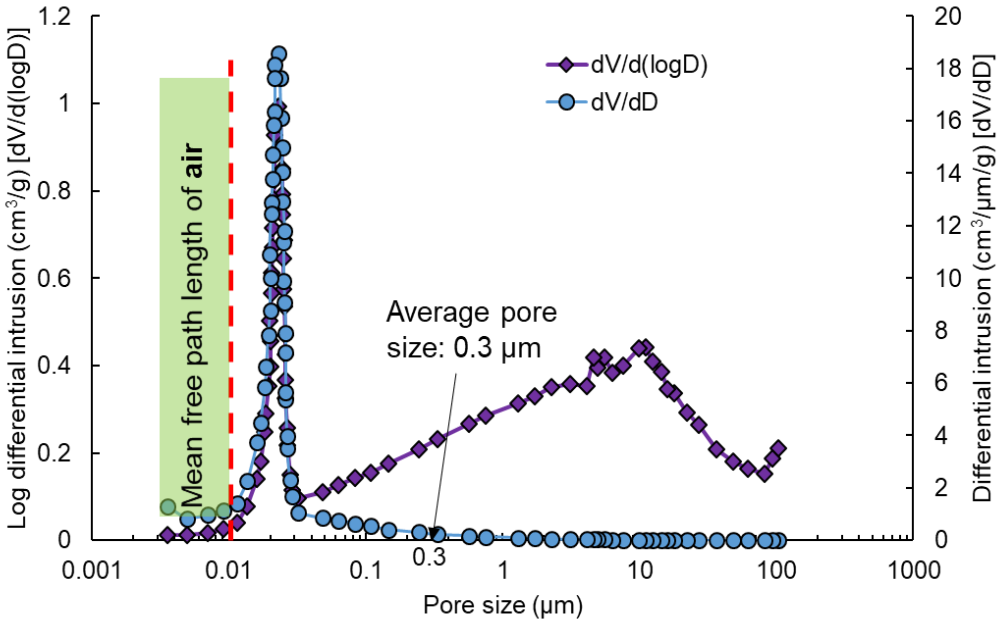

Fig. 8: Pore size distribution of fumed silica with mean free path length of air.

(Kaganer, 1969).

2.2. Design properties

2.2.1. Effect of compaction density / external pressure

To impart mechanical strength to VIPs, core material must be compacted. For instance, fumed silica with a bulk density of 50 kg m^{-3} is compacted to form VIP cores with density of 150-200 kg m^{-3}. Compaction significantly increases the thermal conductivity of the core by increasing the area of contact among neighbouring particles. Fricke et al. (1992, 2008) reported that the variation of solid conductivity with density follows a power law with an exponent of 1.5 for aerogel and 1 for foams. Caps and Fricke (2000) determined that the solid conductivity is a function of external pressure, a measure of density, on a VIP core. They reported the variation of solid conductivity of perlites and precipitated silica. The solid

conductivity of opacified silica powders was found to be approximately proportional to the square root of external pressure and nearly independent of the type of opacifier added. They observed that both the starting point as well as the slope of solid conductivity of perlite core is higher than that of the fumed silica core which indicates that the particle thermal conductivity (k_p) of fumed silica is smaller than that of perlite and that its nano-porous structure is better suited for VIPs. Further, Caps et al. (2001) reported that the solid conductivity of pyrogenic silica is less than that of precipitated silica. The modified phonon model by Bi and Tang (2013) discussed earlier simulated the effect of compaction on the area of contact among particles.

An increase in density results in higher number of radiation attenuating species per unit volume. Therefore, a denser core allows less radiation to pass through as compared to a loose core for the same thickness. As a corollary, it can be said that an increase in the density of the core decreases the radiative conductivity. It is important to note that this behaviour is prominent only for highly porous cores. For high density cores with low porosity, the radiation scattering might change from independent scattering to dependent scattering where clusters of particles instead of separate grains act as scatterers of thermal radiation.

In conclusion, with an increase in compaction density, solid conductivity increases

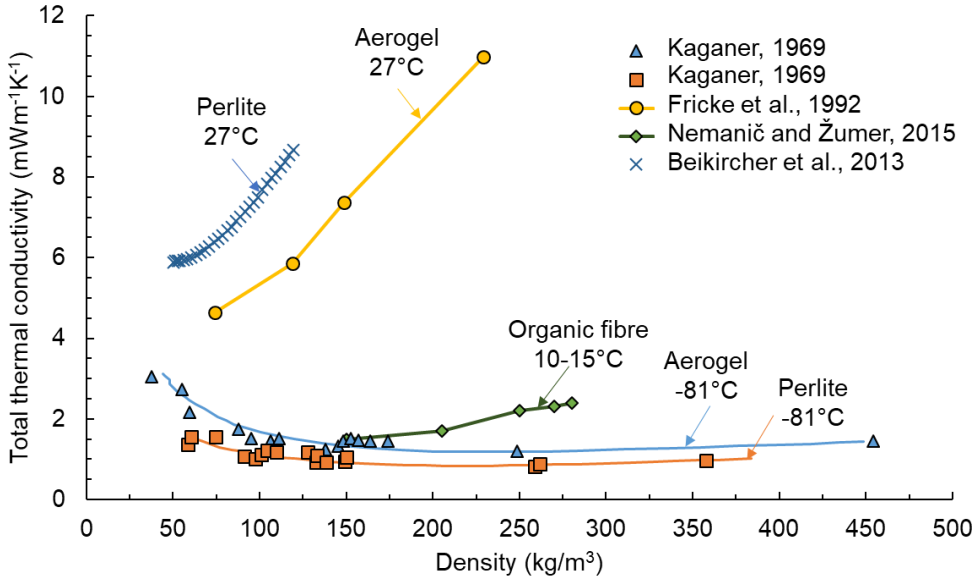

Fig. 9: The effect of density of core material on thermal conductivity of VIP along with the mean temperature of experiments.

exponentially whereas radiative conductivity decreases linearly. Therefore, core density optimisation is important and should be done in conjunction with mechanical strength optimisation for achieving the lowest VIP conductivity. Figure 9 shows the variation of overall thermal conductivity with density for various core materials.

2.2.2. Effect of sealing pressure

Conduction through gas trapped inside the pores is responsible for up to 70-80% of the total thermal conductivity of commonly used insulating materials, excepting VIPs. . Evacuation of this gas could lead to a substantial decrease in the total thermal conductivity.

As discussed earlier, the amount of heat conducted by gas can be controlled by decreasing the pore size of the material. Another (and more efficient) way to restrict gaseous conduction is by evacuating the pores, which results in reducing the heat transferring agents from the pores or significant increase in the mean free path length of gas inside the pores, see equation 11. Figure 10 describes how the mean free path length, shown as red dotted lines, could be increased by application of different vacuum levels.

Figure 11 shows the effect of sealing pressure on VIPs made of several materials. The trends of these values are significantly affected by pore diameter and overall porosity of the core material. For instance, the thermal conductivity of phenolic foam VIP at atmospheric pressure is

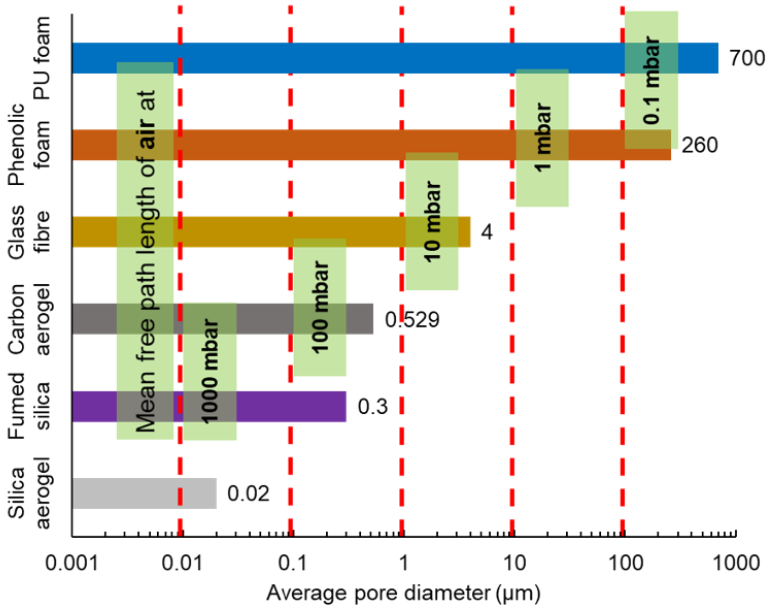

Fig. 10: Effect of pressure on the mean free path length of air in pores.

~30 mW m^{-1} K^{-1} which drops to 5 $mWm^{-1}K^{-1}$ when the gas in its pores is evacuated. This significant change is because of the large pore size of phenolic foam (260 μm). Materials, depending upon their pore sizes, have to be both evacuated to as well as maintained at specific vacuum pressure to deliver an assured VIP thermal conductivity over a full useful life. For simplicity, a critical pressure ($p_{1/2}$) is usually defined as the core pressure at which the total thermal conductivity becomes half of the total conductivity at atmospheric pressure (equation 12). Higher is $p_{1/2}$ of a material, lesser is the sensitivity of its thermal conductivity to pressure change. The calculated values of $p_{1/2}$ of various materials shown in figure 11 are calculated by the authors using a fitting technique and are listed in table 2. The $p_{1/2}$ was determined to be the highest for fumed silica cores due to their lowest pore size. In general, the value of $p_{1/2}$ is highest for powders followed by fibres and foams.

$$l_g = \frac{k_B T}{\sqrt{2}\pi d_g^2 p} \#(11)$$

$$k_g = \frac{k_g^0}{1 + \frac{p_{1/2}}{p}} \#(12)$$

Table 2: Value of $p_{1/2}$ calculated for various VIP core materials

Source	Material	$p_{1/2}$ (mbar)
Caps et al. (2001)	Pyrogenic silica (or fumed silica)	630
Alam et al. (2014)	Expanded perlite composite	330
Chen et al. (2015)	Glass fibre (length: 5.2 μm)	5
Kim et al. (2012)	Phenolic foam	0.8
C. Li et al. (2016)	Hollow glass microspheres composite	70
Nemanič and Žumer (2015)	Organic fibres	25
Caps and Fricke (2000)	Precipitated silica	140

There is negligible change in solid conductivity or in radiative conductivity due to a change in sealing pressure. This information could be employed to derive the values of gaseous conductivity with varying sealing pressure.

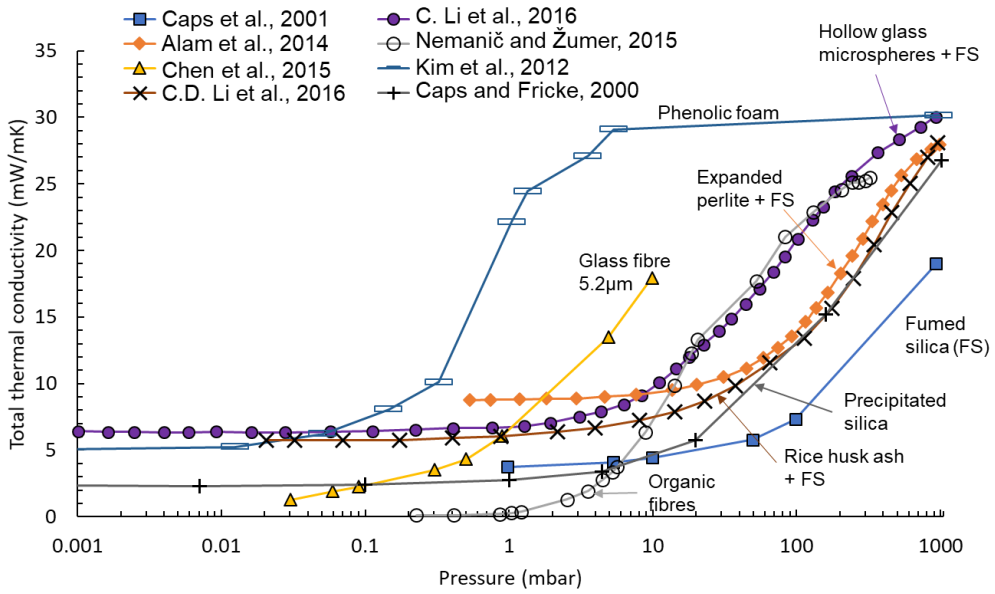

Fig. 11: The effect of VIP sealing pressure on its thermal conductivity.

2.3. Conditions of operation

2.3.1. Effect of the mean operating temperature

The mean operating temperature for a VIP is calculated as the average of the temperatures on its two sides. For refrigerator applications, this mean operating temperature is in the range of 10 °C near the side walls to 50 °C near the compressor area. The heat transfer by radiation is significantly affected as the temperature rises (cubic increase as shown in equation 2). Also, the extinction coefficient decreases with temperature rise, which further increases the heat

transferred through radiation. Radiation significantly contributes to thermal conductivity at elevated temperatures.

Solid conductivity has been found to be a weak function of temperature. For example, solid conductivity of SiO_2 particles has been found to increase from 3 mW m^{-1} K^{-1} at 27 °C to 3.6 mW m^{-1} K^{-1} at 300 °C (Caps et al., 2001). Further, Caps et al. (2001) assumed that the variation in the solid thermal conductivity of silica powders with temperature is proportional to that of the bulk material where powder comes from i.e. glass, given by equation (13).

$$k_s = A[(-8.5E-12)*T^4 + (2.1E-8)*T^3 - (1.95E-5)*T^2 + 0.00883*T] \#(13)$$

The gas molecules inside the pores gain energy due to increase in temperature, thereby increasing their mean free path length (equation 11). This causes a potential decrease in heat transferred by gaseous conduction. However, the thermal conductivity of free gas is also a function of temperature and increases with temperature rise, see equation 14 (Stephan and Laesecke, 1985). Applying the gaseous conductivity prediction models discussed above, it can be concluded that the resultant gaseous conductivity decreases (almost negligibly) with temperature rise at low pressures (<100 mbar) whereas at higher pressures (>100 mbar) it rises.

$$k_{gR}^0 = 33.97T_R^{-1} - 164.7T_R^{-2/3} + 262.1T_R^{-1/3} - 21.5 - 443.4T_R^{1/3} + 607.34T_R^{2/3} - 368.79T_R + 111.29T_R^{4/3} - 13.417T_R^{5/3} \#(14)$$

The temperature dependence of the thermal conductivity of a fumed silica VIP (opacified with 15% SiC) has been studied by Fantucci et al. (2019). They measured a 53% rise in thermal conductivity, from 4.9 mW m^{-1} K^{-1} to 7.5 mW m^{-1} K^{-1}, for a 32 months old fumed silica VIP when temperature was increased from -7.5 °C to 55.5 °C. By performing similar tests on non-evacuated fumed silica boards, they concluded that around 62% (1.6 mW m^{-1} K^{-1}) of this change was due to increase in radiative conductivity and the rest 38% due to the

increase of overall gaseous conductivity with temperature, but the reason for this increase cannot be justified with any of the present gaseous conductivity models. Several studies

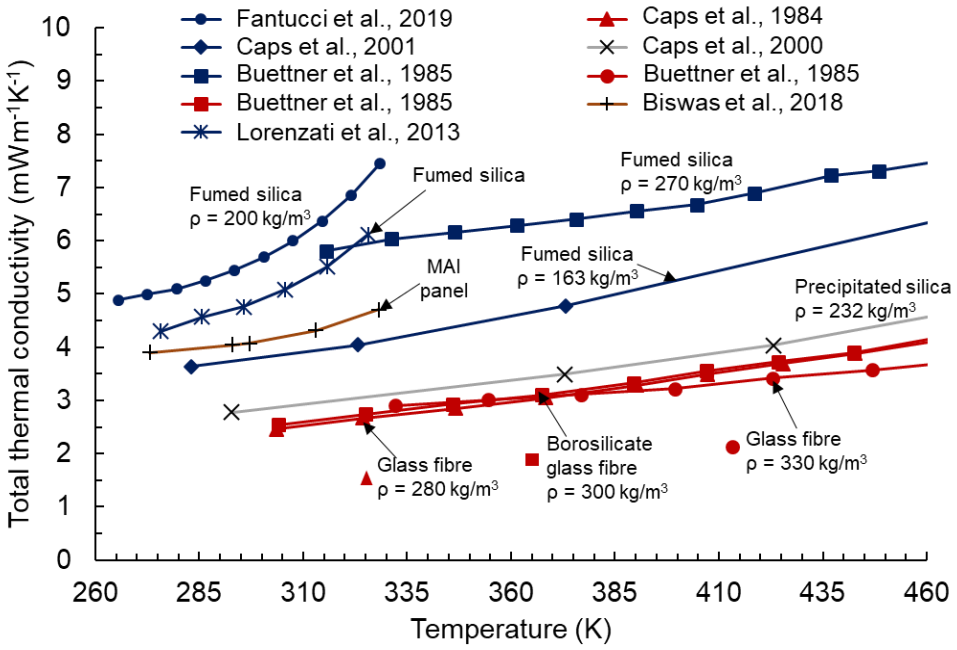

Fig. 12: The effect of mean operating temperature on VIP's thermal conductivity. MAI: modified atmosphere insulation.

which show the effect of temperature on thermal conductivity of fumed silica, glass fibre and MAI VIPs are compiled in figure 12. In general, the thermal conductivity increases with increasing temperature. A major part of this increase is due to increase in radiative conductivity.

2.3.2. Effect of moisture in core

Due to molecular diffusion and mass transmission of water vapour through micro or larger cracks in a damaged envelope, moisture accumulates inside the VIP core. The absorbed or adsorbed water vapour affects the VIPs by i) increasing the overall inner pressure due to partial pressure exerted by water vapour, ii) increasing the overall thermal conductivity due to conduction and radiation by water molecules, iii) changing the pore structure of core material by facilitating agglomeration of particles and thus affecting the solid conductivity and ageing

behaviour (Caps and Fricke, 1986; Pons et al., 2018; Schwab et al., 2005; Simmler and Brunner, 2005). These phenomena are discussed in detail in Section 5.2. Apart from this, presence of moisture inside the core increases the evacuation time significantly. For example, 2% moisture by mass in a 100 g core material at atmospheric pressure translates to approximately 3 litres of water vapour at atmospheric pressure and 30,000 litres of water vapour at 0.1 mbar pressure. A vacuum pump evacuating at a rate of 300 lpm, will take a minimum 1.5 hours to evacuate the core.

3. Alternative core materials for VIPs

Various types of core and envelope materials along with their properties have been discussed by Alam et al. (2011) and Kalnæs and Jelle (2014). Fumed silica, glass fibres and foams have been widely used as VIP cores. To improve cost effectiveness and ageing properties of VIPs researchers have proposed several alternative core materials. This change in material causes a change in the material properties as discussed in section 2.1. The thermo-physical properties of VIPs made with alternative core materials are listed in table 3.

Table 3: Thermo-physical properties of various alternative core materials.

Source	Core material		VIP Thermal conductivity (mW m^{-1} K^{-1})	Pressure (mbar)	VIP Density (kg m^{-3})	Pore size (μm) {Porosity %}
	Primary core	Opacifier				
Kim et al. (2012)	Phenolic foam		5	0.01		260
Alam et al. (2014)	30% Expanded perlite + 50% Fumed silica + 8% Polyester fibre	12% SiC	7.6	0.5	167	0.155 {83}

Nemanič and Žumer (2015)	Organic Melamine-formaldehyde fibres		2.3	<0.001	270	10-100 {81}
Singh et al. (2015)	75% Fumed silica + 5% glass fibre	20% Carbon black	3.7	0.5	183.1	0.4
Chen et al. (2015)	Super stratified glass fibre		2.04	0.09	238	<10
C. Li et al. (2016)	26% Hollow Glass Microfibre + 60% FS + 8% Polyester fibre + 1% Titanium Dioxide	5% Carbon Black	7.2	<1	170	0.173 {88.1}
Chang et al. (2016)	70% Diatomeceous Earth + 30% FS		10.3	1.8	290	{87%}
C. D. Li et al. (2016)	36% RHA + 50% Fumed silica + 8% Polyester fibre + 1% Titanium Dioxide	5% Carbon Black	6.2	<1	114	0.82 {83.7}
Zhuang et al. (2017)	50% Expanded cork + 50% Fumed Silica		6.3	1	200-250	-

4. VIP Lifetime

Mostly, the reported thermal conductivity of VIPs is based on the centre of panel value measured within 1-100 days of manufacturing and the long-term classifications, such as energy saving potential and energy labelling, are calculated using these values. However, it is important to note that thermal conductivity of VIPs increases with time. The rise in

conductivity is caused by two major factors namely pressure rise (leading to gaseous conductivity rise as equation 3) and moisture level rise inside a VIP. Assuming these contributions to be in a parallel resistance network, the total thermal conductivity after time t can be written in the form of equation 15 (Schwab et al., 2005).

$$k(t) = k_{evac} + k_g\big(p(t)\big) + k_w\big(X_w(t)\big) \#(15)$$

If the rate of increase of pressure with time, $p(t)$, is known, $k_g(p)$ can be calculated using any gaseous conductivity model (equations 3-8). Similarly, if the time rate of increase of moisture $X_w(t)$ is known, $k_w(X_w)$ can be approximated as a linear function, see equation (16)

$$k_w(X_w) = bX_w \#(16)$$

Where b is a proportionality constant and is reported for fumed silica to be 0.5 mW m^{-1} K^{-1}/mass% (X_w<10 mass%).

One way to calculate the aged *k*-value is by measuring the pressure and mass increase of the VIP with time and employing equation (3, 15 and 16). The pressure increase due to air and water vapour diffused and permeated through a VIP envelope can be measured using foil lift-off technique or by putting radio frequency identification sensors inside VIPs during manufacturing (Alam et al., 2011). Usually, an assumption is made that the pressure increase is caused solely by permeated dry air ignoring the contribution of water vapours, which should also be accounted for. The amount of moisture permeated to the interiors of a VIP is assessed by simply weighing however this approach is limited to detachable VIPs.

If the Air Transmission Rate (ATR) and Water/Moisture Vapor Transmission Rate ($W/MVTR$) of the envelope are known, the dry air pressure rises and the moisture content inside a VIP can be calculated using equations (17) and (18) (Schwab et al., 2005).

$$p_{air}(t) = \frac{ATR}{V_{eff}}\left(\frac{T_m \cdot p_0}{T_0}\right) * t + p_i \#(17)$$

$$X_w(t) = C\varphi_o\left(1 - \exp\left(\frac{-t \cdot WVTR}{m_{VIP,dry} \cdot C \cdot \varphi_o}\right)\right)\#(18)$$

Where C is the proportionality constant for the linear relationship between the moisture content (X_w) and ambient relative humidity (φ_o) in the envelope core space and can be derived from sorption isotherm.

Equation 16 accounts for reduction in permeation rate as the partial pressure of water inside core builds up, without which the moisture content is known to be over-predicted by 34% for silica core (Simmler and Brunner, 2005).

Equation (15) can be re-written as equation (19).

$$\lambda(t) = \lambda_{evac} + \frac{k_g^0}{1 + \frac{0.032}{D_{mean} \cdot \left(\frac{ATR}{V_{eff}} * t + p_i\right)}} + b * \left(C\varphi_o\left(1 - \exp\left(\frac{-t \cdot WVTR}{m_{VIP,dry} \cdot C \cdot \varphi_o}\right)\right)\right)\#(19)$$

It is important to note that ATR and WVTR are functions of operating temperature, ambient humidity and geometric dimensions of the VIP. Schwab et al. (2005) experimentally calculated the ATR and WVTR of three different envelopes, laminated Aluminium foil (AF) and two Aluminium coated multi-layer foils (MF1 and MF2), at 23 °C/15% RH and 23 °C/75% RH, to calculate the aged thermal conductivity of silica based VIPs. Their results indicated that the increase of *k*-value after 25 years in AF VIPs due to air and moisture penetration was much smaller (0.54 mW m^{-1} K^{-1}) than the MF VIPs (2.4 mW m^{-1} K^{-1}) and hence a longer lifetime was predicted for the former (figure 13).

For a VIP with glass fibre chopped strands as core, the service life (the time in which the thermal resistivity of VIP becomes lower than 87 mK W^{-1}) was estimated to be five years (Di

et al., 2014). As discussed earlier, due to large pore sizes, the thermal conductivity of glass fibre based cores will rise rapidly with increase in core gas pressure. The rise in gaseous conductivity is a dominant factor in glass fibre cores (due to its large pore size) and moisture level increases in fumed silica cores (due to its micro-porous structure) are responsible for the increase in VIP thermal conductivity.

In the case of refrigerators, the temperature and humidity in the vicinity of a refrigerator keep

varying due to compressor function and door openings. A cyclic variation of temperature and humidity increases the ageing effect of VIPs as shown by (Simmler and Brunner, 2005).

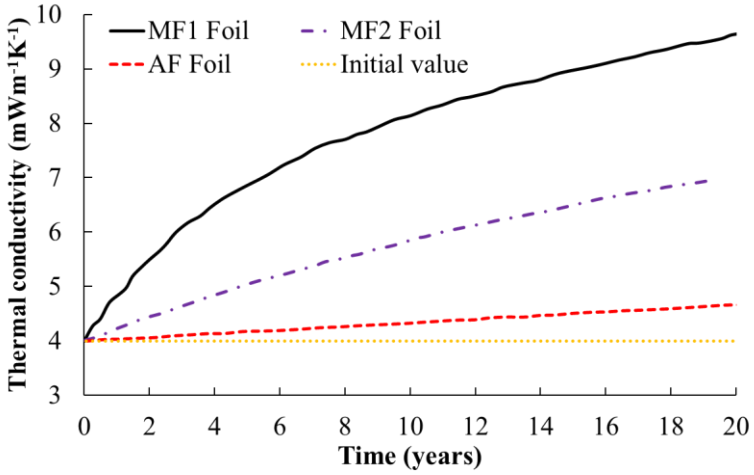

Fig. 13: Thermal conductivity values predicted for 50x50x1 cm^3 VIPs. Adapted from (Schwab et al., 2005).

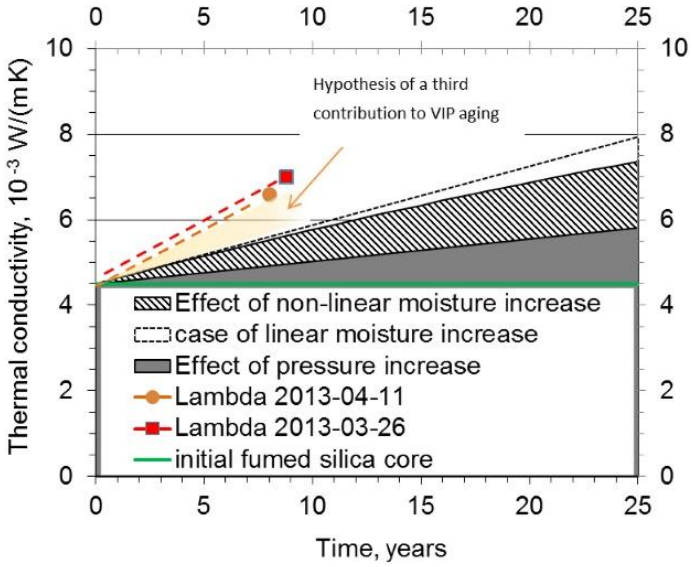

Fig. 14: The real increase in thermal conductivity in 5 years compared with the predicted value (Brunner and Wakili, 2014).

Recent studies (Brunner and Wakili, 2014; Pons et al., 2018) have reported an additional mechanism of ageing, which occurs due to change in the structure of core material due to absorption of moisture, see figure 14. Nonetheless, the results show how the *k*-value changes over the lifespan of a refrigerator which can lead to a significant change in Energy Efficiency Index. To avoid miscommunication, it is important that the insulation and refrigerator manufacturers and regulating agencies should consider ageing while labelling products.

5. Commercial VIPs

Thermal conductivity of a VIP determines the efficiency of energy use of a refrigerator component. Commercial manufacturers invariably quote centre of panel thermal conductivity; see table 4, whereas VIP total thermal conductivity accounts for both, heat transferring normally through the VIP core and that conducted along the envelope material. The latter is referred to as thermal bridging effect. Commercially available VIPs with their reported characteristics are detailed in table 4.

Table 4: Commercially available VIPs and their properties

Manufacturer	Centre of panel thermal conductivity (mW m^{-1} K^{-1})	Comment	Source
BJS Tech	≤ 2	Fumed silica + glass fibre, density: 180-220 kg m^{-3}, thickness: 10-35 mm, length = 100-1800 mm, width: 100-800 mm, temperature stability: -50 °C to 70 °C	(Tech, 2019)
SUPERVAC	2.1	Pressure ≤ 1 mbar; glass fibre, Variant shapes available, 250 – 350 kg m^{-3}, temperature range: -50 °C to 80 °C, thickness: 8mm – 40 mm	(Green Insulator Co Ltd, n.d.)
Fujian SuperTech Advanced Material Co. Ltd.	2.5	240-315 kg m^{-3}, temperature range: -50 °C to 70 °C	(Fujian SuperTech Advanced Material Co Ltd, n.d.)
Thermal Vision	2.88	Pressure = 0.065 mbar; 23.89 °C, 256 kg m^{-3}	(Thermalvisions, n.d.)
U-Vacua	2	(R60/inch), glass fibre + adsorbent, temperature range: -40 °C to 60 °C, 222-240 kg m^{-3},	(Panasonic, n.d.)
TURVAC fg	3.5	Glass fibre core, service life: <15 years' service life 270±20 kg m^{-3}, temperature range: -70 °C to 80 °C	(Turvac, n.d.)
LG Hausys - Fumed Silica	4	160-220 kg m^{-3}, Fumed Silica	(LG Hausys, n.d.)
LG Hausys - Glass Fibre	2.5	220-300 kg m^{-3}, Glass Fibre	(LG Hausys, n.d.)
Vacupor NT	4.1	Pressure = 1 mbar, 22.5 °C, 150-300 kg m^{-3}, standard evacuation pressure: 0.5 mbars	(Porextherm, n.d.)
Microtherm SlimVac	4.2	Pressure < 5mbar, 10 °C, filament reinforced opacified silica, 160-220 kg m^{-3}	(Microthermgroup, n.d.)
TURVAC Si	4.5	Pressure <5mbar; fumed silica core, 40-60 years' service life; 180±20 kg m^{-3}, temperature range:	(Turvac, n.d.)

		-70 °C to 80 °C, 40-60 years' service life	
Kevothermal	4.4	R40 per inch, opacified amorphous silica	(Kevothermal, n.d.)
RPARTS Refrigeration parts solutions	4.4	R40 per inch	(RPARTS, 2019)
OCI Enervac	4.5	40 years' service life, 210±30 kg m^{-3}, Fumed Silica, 5mm – 50 mm	(OCI, n.d.)
va-Q-vip	<5	≤5mbar, pressure rise: <1.5mbar per year; 180-250 kg m^{-3}; pressed powder made of silicic acid, temperature range: -70 °C – 80 °C	(Va-q-tec, n.d.)
va-Q-plus	3.5	<7mbar, rise: <5mbar per year; 160-230 kg m^{-3}; Opacified fumed silica and organic fibres, temperature range: -70 °C – 80 °C	(Va-q-tec, n.d.)
OPTIM-R	7	Includes the effect of both thermal bridging and ageing, thickness: 20 - 50 mm, length: 300 – 1200 mm, width: 300 - 600 mm.	(Kingspan, n.d.)

Commercial VIPs comprise of core made of either glass fibre (LG Hausys, n.d.; Green Insulator Co Ltd, n.d.; Fujian Supertech Advanced Material Co Ltd, n.d.; Panasonic, n.d.; Thermalvisions, n.d.; Turvac, n.d.) or silica powder (Kevothermal, n.d.; Microthermgroup, n.d.; OCI, n.d.; Porextherm, n.d.; RPARTS, 2019.; Turvac, n.d.; Va-q-tec, n.d.). From table 4, one could conclude that glass fibre core VIPs, though reported to achieve a lower centre of panel thermal conductivity (2-3 mW m^{-1} K^{-1}) than fumed silica VIPs (4-6 mW m^{-1} K^{-1}), require up to two orders lower core pressure (<0.01mbar) than FS VIPs (~0.5 mbars). Glass fibre core VIPs suffer from a shorter lifespan whilst being heavier (density 220 – 250 kg m^{-3}) than FS VIPs (density 180-200 kg m^{-3}). Mostly, VIPs are available in oblong shapes, 300 – 1800mm long, 300 – 1200mm wide and 5-50mm thick. Some three dimensionally shaped VIPs, L or cylindrical, are available as well.

6. Conclusions and future challenges

The European Union (EU) has set new targets for energy efficiency, such as at least 32.5% reduction in energy consumption by 2030, following on from the existing 20% target by 2020. With an energy consumption of approximately 14% per household and 6% of the

energy worldwide, refrigerators with improved efficiency could be potential energy savers. VIPs, due to their low thermal conductivity (k<7 $mWm^{-1}K^{-1}$), are key to improve energy efficiency in refrigerators. The Energy Efficiency Index of a refrigerator could change from A+ to A+++ with the application of VIPs, which translates to a saving of approximately 240 kWh_p per year.

Solid conductivity (2-6 mW m^{-1} K^{-1}), a major contributor to total VIP thermal conductivity, depends on the specific core material properties such as the bulk thermal conductivity, elastic modulus, particle size distribution, packing order and density. Glass fibre cores have a low solid conductivity due to a more tortuous heat transfer path offered by the packing arrangement of fibres. Compressive forces exerted during core manufacture result into increasing the area of contact between fibres/particles causing a rise in solid conductivity.

Gaseous conductivity (approximately 5-15 mW m^{-1} K^{-1} in unevacuated cores), which depends on the pore size and porosity of the material, can be significantly suppressed by evacuation up to lower than 0.5 mW m^{-1} K^{-1} depending on core material characteristics. Sufficiently high porosity is desirable for easy evacuation of the core whereas smaller pore sizes are more desirable for a longer service life. To date studies have not explicitly reported the effect of temperature on the gaseous conductivity.

Radiative conductivity (approximately 4 mW m^{-1} K^{-1} for un-opacified cores) can be controlled by addition of opacifiers, such as carbon black or SiC, to <0.5 mW m^{-1} K^{-1}. However, addition of opacifier could invite a penalty in terms of rise in the solid thermal conductivity of the core due to a likely increase in its density. Hence an optimisation of the core material composition is recommended. The mean temperature of the VIP significantly affects the radiative conductivity.

The core accounts for the majority of the total VIP cost. Fumed silica, glass fibres and foams have been widely used as VIP cores in both research and commercial products. Development of cheaper and more durable core materials is one of the major areas of research in VIPs. Alternative core materials have been developed either as composites of cheaper materials with the conventional ones or with a variation in the manufacturing techniques altering the material properties, to reduce the cost of VIPs and improve their ageing properties. Cost is also expected to reduce through economy of scale. The optimisation to identify the best core material from a very large number of potential candidates cannot be realized through lengthy and expensive experiments. Computer modelling of the complex heat transfer phenomenon is necessary to develop newer core composites and envelopes leading to the most cost effective and longest useful life VIP. A comprehensive understanding of these parameters leading to the development of the more cost-effective VIPs would increase their use by enabling the uptake of VIPs in refrigerators and several other similar domestic and industrial gadgets.

References

Alam, M., Singh, H., Brunner, S., Naziris, C., 2014. Experimental characterisation and evaluation of the thermo-physical properties of expanded perlite - Fumed silica composite for effective vacuum insulation panel (VIP) core. Energy Build. 69, 442–450. https://doi.org/10.1016/j.enbuild.2013.11.027

Alam, M., Singh, H., Limbachiya, M.C., 2011. Vacuum insulation panels (vips) for building construction industry - a review of the contemporary developments and future directions. Appl. Energy 88, 3592–3602. https://doi.org/10.1016/j.apenergy.2011.04.040

ASHRAE, 2006. 2006 ASHRAE Handbook: Refrigeration. ASHRAE.

Beikircher, T., Demharter, M., 2013. Heat Transport in Evacuated Perlite Powders for Super-Insulated Long-Term Storages up to 300 °C. J. Heat Transfer 135, 051301. https://doi.org/10.1115/1.4023351

Bi, C., Tang, G.H., 2013. Effective thermal conductivity of the solid backbone of aerogel. Int. J. Heat Mass Transf. 64, 452–456. https://doi.org/10.1016/j.ijheatmasstransfer.2013.04.053

Bi, C., Tang, G.H., Tao, W.Q., 2012. Prediction of the gaseous thermal conductivity in aerogels with non-uniform pore-size distribution. J. Non. Cryst. Solids 358, 3124–3128. https://doi.org/10.1016/j.jnoncrysol.2012.08.011

Biswas, K., Desjarlais, A., Smith, D., Letts, J., Yao, J., Jiang, T., 2018. Development and thermal performance verification of composite insulation boards containing foam-encapsulated vacuum insulation panels. Appl. Energy 228, 1159–1172. https://doi.org/10.1016/j.apenergy.2018.06.136

BJS Tech. Vacuum Insulation Panels [WWW Document]. URL http://www.vacuumisolation.com/vacuum-insulation-panel/ultra-thin-vacuum-insulation-panels-used-in.html (accessed 1.15.19).

Brunner, S., Wakili, K.G., 2014. Hints for an additional aging factor regarding the thermal performance of vacuum insulation panels with pyrogenic silica core. Vacuum 100, 4–6. https://doi.org/10.1016/j.vacuum.2013.07.033

Buettner, D., Fricke, J., Reiss, H., 1985. Analysis of radiative and solid conduction components of the total thermal conductivity of an evacuated glass fiber insulation measurements with a 700 x 700 sq mm variable load guarded hot plate device, in: AIAA 20th Thermophysics Conference. Williamsburg Virginia. https://doi.org/10.2514/6.1985-1019

Caps, R., Fricke, J., 2000. Thermal conductivity of opacified powder filler materials for vacuum insulations. Int. J. Thermophys. 21, 445–452. https://doi.org/10.1023/A:1006691731253

Caps, R., Fricke, J., 1986. Infrared radiative heat transfer in highly transparent silica aerogel. Sol. Energy 36, 361–364. https://doi.org/10.1016/0038-092X(86)90153-2

Caps, R., Heinemann, U., Ehrmanntraut, M., Fricke, J., 2001. Evacuated insulation panels filled with pyrogenic silica powders: Properties and applications. High Temp. - High Press. 33, 151–156. https://doi.org/10.1068/htwu70

Caps, R., Trunzer, A., Büttner, D., Fricke, J., Reiss, H., 1984. Spectral transmission and reflection properties of high temperature insulation materials. Int. J. Heat Mass Transf. 27, 1865–1872. https://doi.org/10.1016/0017-9310(84)90168-6

Chang, B., Zhong, L., Akinc, M., 2016. Low cost composites for vacuum insulation core material. Vacuum 131, 120–126. https://doi.org/10.1016/j.vacuum.2016.05.027

Chen, Zhou, Chen, Zhaofeng, Yang, Z., Hu, J., Yang, Y., Chang, L., Lee, L.J., Xu, T., 2015. Preparation and characterization of vacuum insulation panels with super-stratified glass fiber core material. Energy 93, 945–954. https://doi.org/10.1016/j.energy.2015.08.105

Di, X., Gao, Y., Bao, C., Ma, S., 2014. Thermal insulation property and service life of vacuum insulation panels with glass fiber chopped strand as core materials. Energy Build. 73, 176–183. https://doi.org/10.1016/j.enbuild.2014.01.010

Deissler, R.G., 1964. Diffusion approximation for the thermal radiation in gases with jump boundary condition. ASME J. heat Transf. 86, 240–246. https://doi.org/https://doi.org/10.1115/1.3687110

Fantucci, S., Lorenzati, A., Capozzoli, A., Perino, M., 2019. Analysis of the temperature dependence of the thermal conductivity in Vacuum Insulation Panels. Energy Build. 183, 64–74. https://doi.org/10.1016/j.enbuild.2018.10.002

Fricke, J., Lu, X., Wang, P., Büttner, D., Heinemann, U., 1992. Optimization of monolithic silica aerogel insulants. Int. J. Heat Mass Transf. https://doi.org/10.1016/0017-9310(92)90073-2

Fujian Supertech Advanced Materials Co Ltd. Vacuum Insulation Panel [WWW Document]. URL https://fjsupertech.en.ecplaza.net/products/vacuum-insulation-panel_3546642 (accessed 1.15.19).

Green Insulator Co Ltd. Supervac [WWW Document]. URL http://supervac.koreasme.com/introduction.html (accessed 1.15.19).

Hammond, E.C., Evans, J.A., 2014. Application of Vacuum Insulation Panels in the cold chain - Analysis of viability. Int. J. Refrig. 47, 58–65. https://doi.org/10.1016/j.ijrefrig.2014.07.010

IIR, 2009. COP 15 Copenhagen. Copenhagen, Denmark.

LG Hausys. Vacuum Insulation Panel [WWW Document]. URL http://www.lghausys.com/business/ITElectronics/vip.jsp?gubun=product&pid=41(accessed 1.15.19).

Kaganer, M., 1969. Thermal insulation in cryogenic engineering.

Kalnæs, S.E., Jelle, B.P., 2014. Vacuum insulation panel products: A state-of-the-art review and future research pathways. Appl. Energy 116, 355–375. https://doi.org/10.1016/j.apenergy.2013.11.032

Kevothermal. Stationary refrigeration [WWW Document]. URL http://kevothermal.com/stationary_refrigeration.html (accessed 1.15.19).

Kim, J., Lee, J.H., Song, T.H., 2012. Vacuum insulation properties of phenolic foam. Int. J. Heat Mass Transf. 55, 5343–5349. https://doi.org/10.1016/j.ijheatmasstransfer.2012.05.051

Kingspan. Insulation [WWW Document]. URL https://az750602.vo.msecnd.net/netxstoreviews/assetOriginal/22129_ProductBrochure_OPTIM-R_UK.pdf (accessed 1.15.19).

Kuhn, J., Ebert, H.P., Arduini-Schuster, M.C., Buttner, D., Fricke, J., 1992. Thermal transport in polystyrene and polyurethane foam insulations. Int. J. Heat Mass Transf. 35, 1795–1801. https://doi.org/10.1016/0017-9310(92)90150-Q

Kwon, J.S., Jang, C.H., Jung, H., Song, T.H., 2009. Effective thermal conductivity of various filling materials for vacuum insulation panels. Int. J. Heat Mass Transf. 52, 5525–5532. https://doi.org/10.1016/j.ijheatmasstransfer.2009.06.029

Lee, O.J., Lee, K.H., Jin Yim, T., Young Kim, S., Yoo, K.P., 2002. Determination of mesopore size of aerogels from thermal conductivity measurements. J. Non. Cryst. Solids. https://doi.org/10.1016/S0022-3093(01)01041-9

Li, C., Li, B., Pan, N., Chen, Z., Saeed, M.U., Xu, T., Yang, Y., 2016. Thermo-physical properties of polyester fiber reinforced fumed silica/hollow glass microsphere composite core and resulted vacuum insulation panel. Energy Build. 125, 298–309. https://doi.org/10.1016/j.enbuild.2016.05.013

Li, C.D., Saeed, M.U., Pan, N., Chen, Z.F., Xu, T.Z., 2016. Fabrication and characterization of low-cost and green vacuum insulation panels with fumed silica/rice husk ash hybrid core material. Mater. Des. 107, 440–449. https://doi.org/10.1016/j.matdes.2016.06.071

Liang, Y., Wu, H., Huang, G., Yang, J., Ding, Y., 2017. Prediction and Optimization of

Thermal Conductivity of Vacuum Insulation Panels with Aerogel Composite Cores. Procedia Eng. 205, 2855–2862. https://doi.org/10.1016/j.proeng.2017.09.909

Lorenzati, A., Fantucci, S., Capozzoli, A., Perino, M., 2015. VIPs thermal conductivity measurement: Test methods, limits and uncertainty. Energy Procedia 78, 418–423. https://doi.org/10.1016/j.egypro.2015.11.686

Microthermgroup. Microtherm SlimVac [WWW Document]. URL https://www.bagges.no/wp-content/uploads/2016/02/Teknisk-datablad-Microtherm®-SlimVac.pdf (accessed 1.15.19).

Napp, V., Caps, R., Ebert, H.P., Fricke, J., 1999. Optimization of the thermal radiation extinction of silicon carbide in a silica powder matrix. J. Therm. Anal. Calorim. 56, 77–85. https://doi.org/10.1023/A:1010131324100

Negrão, C.O.R., Hermes, C.J.L., 2011. Energy and cost savings in household refrigerating appliances: A simulation-based design approach. Appl. Energy 88, 3051–3060. https://doi.org/10.1016/j.apenergy.2011.03.013

Nemanič, V., Žumer, M., 2015. New organic fiber-based core material for vacuum thermal insulation. Energy Build. 90, 137–141. https://doi.org/10.1016/j.enbuild.2015.01.012

OCI. VIP [WWW Document]. URL https://www.oci.co.kr/eng/sub/business/vip.asp (accessed 1.15.19).

Panasonic, n.d. U-Vacua [WWW Document]. URL https://na.industrial.panasonic.com/sites/default/pidsa/files/downloads/files/panasonic-vip-uvacua-datasheet.pdf (accessed 1.15.19).

Placido, E., Arduini-Schuster, M.C., Kuhn, J., 2005. Thermal properties predictive model for insulating foams. Infrared Phys. Technol. 46, 219–231. https://doi.org/10.1016/j.infrared.2004.04.001

Pons, E., Yrieix, B., Brunner, S., 2018. Evaluation of VIPs after mild artificial aging during 10 years: Focus on the core behavior. Energy Build. 162, 198–207. https://doi.org/10.1016/j.enbuild.2017.12.016

Porextherm. Vacuum Insulation Panels Vacupor [WWW Document]. URL http://www.porextherm.com/en/products/vacupor/vacupor-nt.html (accessed 1.15.19).

Reichenauer, G., Heinemann, U., Ebert, H.P., 2007. Relationship between pore size and the gas pressure dependence of the gaseous thermal conductivity. Colloids Surfaces A Physicochem. Eng. Asp. 300, 204–210. https://doi.org/10.1016/j.colsurfa.2007.01.020

RPARTS. Vacuum Insulation Panels [WWW Document]. URL http://www.rparts.com/index.php?cPath=84_32&osCsid=seur2sv7fgqnp3k961sopqq7g5 (accessed 1.15.19).

Schwab, H., Heinemann, U., Beck, A., Ebert, H.P., Fricke, J., 2005. Prediction of service life for vacuum insulation panels with fumed silica kernel and foil cover. J. Therm. Envel. Build. Sci. 28, 357–374. https://doi.org/10.1177/1097196305051894

Simmler, H., Brunner, S., 2005. Vacuum insulation panels for building application: Basic properties, aging mechanisms and service life. Energy Build. 37, 1122–1131. https://doi.org/10.1016/j.enbuild.2005.06.015

Singh, H., Geisler, M., Menzel, F., 2015. Experimental investigations into thermal transport phenomena in vacuum insulation panels (VIPs) using fumed silica cores. Energy Build. 107, 76–83. https://doi.org/10.1016/j.enbuild.2015.08.004

Stephan, K., Laesecke, A., 1985. The Thermal Conductivity of Fluid Air. J. Phys. Chem. Ref. Data 227. https://doi.org/http://dx.doi.org/10.1063/1.555749

Tao, W.H., Huang, C.M., Hsu, C.L., Lin, J.Y., 2004. Performance study of an energy-efficient display case refrigerator. Chem. Eng. Commun. 191, 550–565. https://doi.org/10.1080/00986440490277983

Thermalvisions. THRESHHOLD [WWW Document]. URL http://www.thermalvisions.com/Theshhold_page.html (accessed 1.15.19).

Thiessen, S., Knabben, F.T., Melo, C., Goncalves, J.M., 2016. An Experimental Study on the Use of Vacuum Insulation Panels in Household Refrigerators. Int. Compress. Eng. Refrig. Air Cond. High Perform. Build. Conf. 1–8.

Trias, F.X., Oliet, C., Rigola, J., Pérez-Segarra, C.D., 2018. A simple optimization approach for the insulation thickness distribution in household refrigerators. Int. J. Refrig. 93, 169–175. https://doi.org/10.1016/j.ijrefrig.2018.06.014

Turiel, I., Levine, M.D., 1993. Reduction of Chlorofluorocarbon Use.

Turvac. Turvac fg [WWW Document]. URL https://www.turvac.eu/0/Products/TURVACfg.aspx (accessed 1.15.19a).

Turvac. Turvac Si [WWW Document]. URL https://www.turvac.eu/0/Products/TURVACsi.aspx (accessed 1.15.19b).

Va-q-tec. Va-q-vip [WWW Document]. URL https://www.va-q-tec.com/en/produkte/va-q-vip/ (accessed 1.15.19a).

Va-q-tec. Va-q-plus [WWW Document]. URL https://www.va-q-tec.com/en/produkte/va-q-plus/ (accessed 1.15.19b).

Verma, S., Singh, H., 2019a. Why and which insulation materials for refrigerators!, in: International Congress of Refrigeration. Montreal, pp. 1–7. https://doi.org/10.18462/iir.icr.2019.1874

Verma, S., Singh, H., 2019b. Vacuum insulation in cold chain equipment: A review, in: Energy Procedia. https://doi.org/10.1016/j.egypro.2019.02.086

Wang, X.D., Sun, D., Duan, Y.Y., Hu, Z.J., 2013. Radiative characteristics of opacifier-loaded silica aerogel composites. J. Non. Cryst. Solids. https://doi.org/10.1016/j.jnoncrysol.2013.04.058

Webb, P.A., 1993. Data Collection, Reduction and Presentation, Micromeritics Pore Sizer 9320 AutoPore II 9220.

Wei, G., Liu, Y., Zhang, X., Yu, F., Du, X., 2011. Thermal conductivities study on silica aerogel and its composite insulation materials. Int. J. Heat Mass Transf. 54, 2355–2366. https://doi.org/10.1016/j.ijheatmasstransfer.2011.02.026

Y.Yusufoglu, 2013. Application of Vacuum Insulation Panels (VIPs) onRefrigerators, in: Brunner, S., Ghazi Wakili, K. (Eds.), 11th International Vacuum Insulation Symposium. Dubendorf, pp. 21–23.

Zhang, C., Li, J., Hu, Z., Zhu, F., Huang, Y., 2012. Correlation between the acoustic and porous cell morphology of polyurethane foam: Effect of interconnected porosity. Mater. Des. https://doi.org/10.1016/j.matdes.2012.04.031

Zhu, C.Y., Li, Z.Y., Pang, H.Q., Pan, N., 2018. Design and optimization of core/shell structures as highly efficient opacifiers for silica aerogels as high-temperature thermal insulation. Int. J. Therm. Sci. 133, 206–215. https://doi.org/10.1016/j.ijthermalsci.2018.07.032

Zhuang, J., Ghaffar, S.H., Fan, M., Corker, J., 2017. Restructure of expanded cork with fumed silica as novel core materials for vacuum insulation panels. Compos. Part B Eng. 127, 215–221. https://doi.org/10.1016/j.compositesb.2017.06.019